2014

Effect of molecular models on viscosity and thermal conductivity calculations

Andrew B. Weaver

Alina A. Alexeenko
Purdue University - Main Campus, alexeenk@purdue.edu

Recommended Citation

Weaver, Andrew B. and Alexeenko, Alina A., "Effect of molecular models on viscosity and thermal conductivity calculations" (2014). *School of Aeronautics and Astronautics Faculty Publications.* Paper 42.
http://dx.doi.org/10.1063/1.4902582

Effect of Molecular Models on Viscosity and Thermal Conductivity Calculations

Andrew B. Weaver and Alina A. Alexeenko

Purdue University, West Lafayette, IN 47907, USA

Abstract. The effect of molecular models on viscosity and thermal conductivity calculations is investigated. The Direct Simulation Monte Carlo (DSMC) method for rarefied gas flows is used to simulate Couette and Fourier flows as a means of obtaining the transport coefficients. Experimental measurements for argon (Ar) provide a baseline for comparison over a wide temperature range of 100–1,500 K. The variable hard sphere (VHS), variable soft sphere (VSS), and Lennard-Jones (L-J) molecular models have been implemented into a parallel version of Bird's one-dimensional DSMC code, DSMC1, and the model parameters have been recalibrated to the current experimental data set. While the VHS and VSS models only consider the short-range, repulsive forces, the L-J model also includes contributions from the long-range, dispersion forces. Theoretical results for viscosity and thermal conductivity indicate the L-J model is more accurate than the VSS model; with maximum errors of 1.4% and 3.0% in the range 300–1,500 K for L-J and VSS models, respectively. The range of validity of the VSS model is extended to 1,650 K through appropriate choices for the model parameters.

Keywords: DSMC, transport properties, Lennard-Jones, variable soft sphere
PACS: 47.45-n 02.60.Cb 51.20.+d

INTRODUCTION

The use of the direct simulation Monte Carlo (DSMC) method has drastically increased over the years, with applications ranging from micro-electro-mechanical systems [1, 2] (MEMS) to high-energy hypersonic flows [3, 4] over entire vehicles. Simplistic models developed in the late 1970s to early 1980s, such as the variable hard sphere [5] (VHS) and variable soft sphere [6] (VSS) models, are still commonly found in DSMC codes today. Unlike the hard sphere (HS) model, which has a square-root dependence of viscosity on temperature, the VHS and VSS models follow a general power-law viscosity variation with temperature.

Each of these models have limited validity due to the fact that they do not account for the attractive force between molecules at large distances. Also, the model parameters are chosen in such a way that the viscosity variation of the gas under consideration is reproduced only for a relatively narrow range of temperatures. For problems involving a wide range of temperatures, this would be insufficient. Examples include flows with large temperature variations such as supersonic plume expansions in vacuum as encountered in space propulsion and in low-pressure deposition of thin film materials where the vapor temperature varies from the melting point of the material to very low temperatures due to rapid expansion into vacuum. In other applications the detailed collision dynamics that includes the contribution of the attractive interactions between molecules becomes important. For example, this is the case when the orientation of a molecule incident on a solid surface should be accurately predicted along with the incident energy of the molecule for thin film growth modeling.

Higher-fidelity models are available for elastic collision modeling, but they have seen limited use in DSMC owing to the added complexity and computational requirements. In recent years, efficient DSMC implementations of a more physically realistic intermolecular potential, Lennard-Jones (L-J), have been developed. [7, 8] Though the use of such physically realistic models is expected to be more accurate, a thorough comparison of a variety of models in practical engineering applications and their computational advantages is currently lacking. In this work, the effect of the choice of the intermolecular potential on viscosity and thermal conductivity calculations in DSMC is investigated.

The remainder of the paper is organized as follows. The second section on theory and background provides the necessary background about existing DSMC collision models and the LJ potential. A verification of the DSMC implementation of the LJPA model is presented in the third section; while the fourth section presents the viscosity and thermal conductivity calculations using two sets of model parameters for the VSS and LJPA collision models. Finally, concluding remarks are summarized in the last section.

Proceedings of the 29th International Symposium on Rarefied Gas Dynamics
AIP Conf. Proc. 1628, 115-122 (2014); doi: 10.1063/1.4902582

THEORY & BACKGROUND

Purely Repulsive Interaction Models

The various purely repulsive models proposed in the past are briefly summarized below. The single parameter that completely describes an elastic collision between two atoms or molecules by relating the pre-collisional and post-collisional velocities is the scattering angle, χ, which strongly depends on the nature of intermolecular forces between the two molecules. χ depends on the relative energies of the two colliding molecules, $\varepsilon = m_r c_r^2/2$, and the impact parameter, b. In the expression for ε, m_r is the reduced mass, $m_1 m_2/(m_1+m_2)$, for collisions between molecules of mass m_1 and m_2, and c_r is the relative velocity between the colliding molecules. The purely repulsive interaction models result in a scattering angle that is non-negative and lies between 0 and 180°. The scattering angle for the VSS model [5] ,

$$\chi = 2\cos^{-1}\left[\left(\frac{b}{d_{VSS}}\right)^{1/\alpha}\right], \tag{1}$$

is similar in form to the VHS scattering angle, and in fact when α is unity the VHS scattering is obtained. The diameter dependence on relative velocity, d_{VSS}, is also the same as for d_{VHS}. This dependence has the form of,

$$d_{VSS} = d_{VHS} = d_{\text{ref}}\left[\frac{1}{\Gamma(5/2-\omega)}\left(\frac{2kT_{\text{ref}}}{m_r c_r^2}\right)^{(\omega-0.5)}\right]^{1/2}, \tag{2}$$

with the purpose of improving agreement to viscosity measurements. In the previous expression, k is the Boltzmann constant and Γ denotes the Gamma function. The four VSS parameters are: d_{ref} the reference diameter, T_{ref} the reference temperature, ω the viscosity temperature exponent, and the scattering parameter, α. A value of 0.5 for ω corresponds to the HS model, while a value of 1 corresponds to a Maxwell molecule. The variation of viscosity with temperature may be then be predicted in theory according to a power law for both VHS and VSS models as

$$\mu = \mu_{ref}\left(\frac{T}{T_{ref}}\right)^{\omega}. \tag{3}$$

Lennard-Jones Interaction Model

The LJ potential is one of the realistic intermolecular potentials which accounts for both the short-range repulsive and long-range attractive forces between neutral molecules through inverse power laws. Due to the inclusion of the attractive force, the LJ potential,

$$U(r) = 4\varepsilon_{LJ}\left[\left(\frac{\sigma_{LJ}}{r}\right)^{12} - \left(\frac{\sigma_{LJ}}{r}\right)^{6}\right], \tag{4}$$

has a minimum energy denoted by ε_{LJ}. This minimum potential energy along with the intermolecular separation distance corresponding to zero potential energy, σ_{LJ}, constitute the LJ model parameter set. The inclusion of the attractive component also results in negative scattering angles for larger impact parameters.

The viscosity variation with temperature, T, obtained from Chapman-Enskog theory [9, 10] using the LJ potential is

$$\mu = \frac{5}{8\sigma_{LJ}^2}\sqrt{\frac{m_r kT}{2\pi}}\frac{f_\mu^{(Kihara)}}{\Omega^{*(2,2)}}, \tag{5}$$

where m_r is the reduced mass, k is the Boltzmann constant, and $f_\mu^{(Kihara)}$ and $\Omega^{*(2,2)}$ are functions of kT/ε_{LJ} that are, for example, tabulated in the work of Hirschfelder *et al.* [9, 10]. The thermal conductivity may also be computed to first approximation from Chapman-Enskog theory. [5] It may be written as a linear function of viscosity, $k = 15k\mu/4m$, and therefore the thermal conductivity calculations are expected to follow similar trends as for viscosity.

Figure 1 compares the viscosity variation of argon obtained from experiments [11, 12, 13], predictions using the LJ potential [9], the most commonly used VSS model for argon [5] and a curve fit obtained by Maitland and Smith [14] using data from a number of experiments for argon. A similar comparison is illustrated in figure 1 for molecular nitrogen using the Maitland-Smith fit. The Maitland-Smith fit for argon is expected to lead to an error of less than

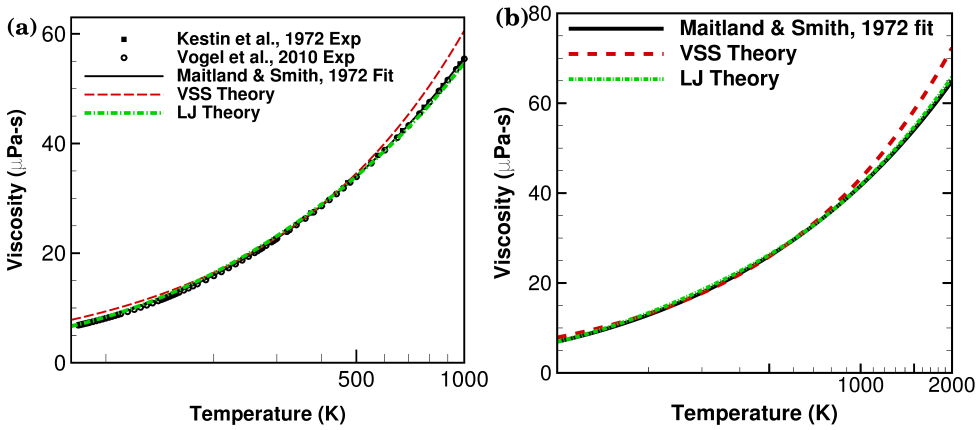

FIGURE 1. Comparison of (a) argon viscosity and (b) molecular nitrogen viscosity obtained using the VSS model [5], LJ potential [9, 10], Maitland-Smith fit [14], and experiments by Kestin et al. [11] and Vogel et al. [13].

1% in the temperature range 80–600 K and 1.5% between 600 and 2,200 K. For molecular nitrogen, these errors are estimated at 1% between 100 and 200 K, 0.5% between 200 and 300 K, and 1.5% between 300 and 2,200 K. As can be seen, the viscosity variation obtained using the LJ potential parameters agrees extremely well with the experiments and the Maitland-Smith curve fit; whereas the VSS model's performance is best near its reference temperature of 273 K. This is mainly due to the fact that the VSS model does not account for the attractive component of the force which becomes important at low temperatures. It should be mentioned that use of a different VSS model in the low- or high-temperature regimes will lead to good agreement with the experimental data, but not necessarily so for a single parameter set.

For the LJ potential, the scattering angle χ may be written as [15]

$$\chi = \pi - 2\sqrt{1+cz-(1+c)z^2}\int_0^1 \{1-[1+cz-(1+c)z^2]u^2+czu^6-(1+c)z^2u^{12}\}^{-1/2}du, \tag{6}$$

where $c=(2/\varepsilon^*)[1+\sqrt{1+\varepsilon^*}]$, $z=(4/c\varepsilon^*)(\sigma_{LJ}/r_0)^6$, and $u=r_0/r$. The distance of closest approach between the two molecules is denoted by r_0; while the reduced relative collision energy is a ratio of the relative collision energy to the LJ potential well depth, $\varepsilon^*=\varepsilon/\varepsilon_{\mathrm{LJ}}$. A reduced form of the impact parameter is also used, where the impact parameter is non-dimensionalized by the intermolecular separation distance of zero energy, $b^*=b/\sigma_{\mathrm{LJ}}$. Varying u from 0 to 1 varies r from ∞ to r_0. z in the above integral depends on b^* and ε^* and is obtained by solving the implicit equation,

$$b^* = \left(\frac{4}{c\varepsilon^*}\right)^{1/6}\sqrt{1+cz-(1+c)z^2}\,z^{-1/6}. \tag{7}$$

The LJ polynomial approximation [8] (LJPA) model simplifies the scattering angle calculations to that of a two-dimensional, seventh-order polynomial of the form,

$$\chi = \sum_{i=0}^{7}\sum_{j=0}^{7-i}\hat{\chi}_{ij}\hat{b}^{*i}\hat{\varepsilon}^{*j}. \tag{8}$$

The two variables, $\hat{b}^{*i}$ and $\hat{\varepsilon}^{*j}$ denote reduced impact parameter and reduced relative collision energy, respectively, while the coefficients are denoted by $\hat{\chi}_{ij}$. Detailed explanations of its implementation and a listing of the required $\hat{\chi}_{ij}$ coefficients are presented in reference [8].

VERIFICATION OF LJPA MODEL

The LJPA model is verified through comparison of equilibrium collision frequencies computed at several temperatures to theory. Equilibrium collision frequency is computed as a product of number density and the mean of the

TABLE 1. LJ Collision Frequencies Computed from DSMC and Theory.

T(K)	ν_{LJPA}(Hz)	ν_{Direct}(Hz)	$\nu_{Theory}(Hz)$	ν_{LJPA} Error (%)	ν_{Direct} Error (%)
40	$25,813.2 \pm 0.1$	$25,812.5 \pm 0.1$	25,808.4	0.019	0.016
273.15	$66,130.7 \pm 0.5$	$66,128.4 \pm 0.3$	66,117.8	0.020	0.016
1,000	$129,090.9 \pm 1.$	$129,085.8 \pm 0.6$	129,084.5	0.005	0.001
1,500	$154,932.6 \pm 0.4$	$154,926.5 \pm 1.$	154,936.4	-0.002	-0.006

product of total cross-section and relative velocity. The mean of the product, $\overline{\sigma_T c_r}$, is averaged over the relative velocity distribution function, f_{c_r}, such that the equilibrium collision frequency has the form [5],

$$\nu_0 = n\overline{\sigma_T c_r} \tag{9}$$

$$= n\int_0^\infty \sigma_T c_r f_{c_r}\,\mathrm{d}c_r \tag{10}$$

$$= 4n\frac{m_r^{3/2}}{\sqrt{\pi}\,(2kT)^{3/2}}\int_0^\infty \left(\pi b_{max}^2\right) c_r^3 \exp\left[-\frac{m_r c_r^2}{2kT}\right]\mathrm{d}c_r\,. \tag{11}$$

The total cross-section for the LJ potential would theoretically extend to infinity, and therefore a maximum impact parameter [6, 8],

$$b_{max} = \sigma_{LJ}\max\left[\left(\frac{4\pi}{\varepsilon^*\chi_{min}}\right)^{\frac{1}{6}}, \left(\frac{6\pi}{\varepsilon^*\chi_{min}}\right)^{\frac{1}{12}}\right], \tag{12}$$

is set to a value beyond which scattering angles less than χ_{min} are neglected. This variation of total cross-section with relative velocity also necessitates the use of numerical integration techniques, such at those described in Ref. [8]. In this section, as well as in the remainder of the paper, a minimum scattering angle of 0.1 radians is used.

The DSMC implementation of the LJ potential itself follows the work of Koura and Matsumoto [15] very closely with the principal difference being the use of the polynomial expansion for the scattering angle [8] instead of a concurrent numerical integration. The DSMC simulations were performed using the one-dimensional code of Bird [5], DSMC1.FOR, after implementation of the LJPA model.

Collision frequencies are computed from DSMC using both the LJPA model and the direct LJ scattering from the integral, Eq. (6). A single cell of length, 1 mm, with 40,000 molecules and a number density corresponding to $Kn = 10$ is used. A time-step of $\tau_0/10$ is used, where τ_0 is the mean collision time as computed from theory ($1/\nu_0$). DSMC sampling speeds of each LJ scattering angle implementation are recorded using a single processor on the Hansen compute cluster. The Hansen compute cluster has four 2.3 GHz 12-Core AMD Opteron 6176 processors per node, 10GB Ethernet interconnections, and 48.8 TeraFLOPS performance. Sampling speeds for the LJPA model ranged from 33.0 samples/s to 39.9 samples/s; while the direct LJ scattering implementation resulted in approximately half the sampling speed of 14.9–15.1 samples/s. Collision frequencies computed from DSMC and theory are reported in table 1 along with their corresponding errors relative to theory.

The statistical errors reported as a two-sided 95% confidence interval are much smaller than the errors in collision frequency relative to theory; thus providing confidence in the results. Both DSMC implementations of the LJ scattering angle have comparable collision frequencies at each of the simulated temperatures, and are in error by less than 0.02%. The good agreement verifies the implementation of the LJPA model in DSMC, and the errors are consistent with those reported for the VHS model at 300 K [16].

VISCOSITY AND THERMAL CONDUCTIVITY CALCULATIONS

Viscosity and thermal conductivity calculations are carried out using the theoretical expressions provided in the second section of theory and background as well as DSMC simulations of Couette and Fourier flows. A description of the 32 cases including input conditions and results is presented in this section. These 32 cases account for both Couette and Fourier flows being simulated in DSMC1 at the 8 nominal temperatures $T_n = 100, 300, 500, \ldots, 1{,}500$ K using both VSS and L-J intermolecular potentials. Couette flow is modeled with two diffuse walls translating in the y-direction at equal and opposite velocities. The velocities were chosen such that they are $\pm 10\%$ of the root mean square

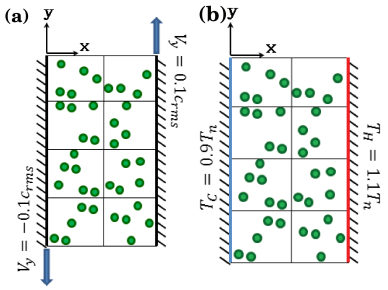

FIGURE 2. Schematics of (a) Couette and (b) Fourier Flows.

TABLE 2. Physical and Numerical DSMC1 input parameters.

Flow Type	T_n(K)	P_{or}(Torr)	Couette Flow $\pm 0.1c_{rms}$(m/s)	Fourier Flow $\pm 0.1T_n$(K)	Time-Step (ns)
Couette & Fourier	100	0.3930	25	10	10.9
	300	1.656	45	30	6.3
	500	3.234	56	50	4.9
	700	5.025	66	70	4.1
	900	6.985	75	90	3.6
	1,100	9.085	83	110	3.3
	1,300	11.31	90	130	3.0
	1,500	13.64	97	150	2.8

(rms) speed, $c_{rms} = (3kT/m)^{1/2}$, and thus result in velocities which increase with increasing temperature. Fourier flow is modeled with two diffuse walls, with the walls being held at constant temperatures that differ by $\pm 10\%$ from the nominal temperature. Both viscosities and thermal conductivities are computed within each sampling cell, and the values reported are averages over the central 60% of the domain in order to exclude the Knudsen layer. Schematics are shown in Fig. 2 for Couette and Fourier flows.

The numerical parameters for discretizing the spatial and temporal terms of the governing Boltzmann equation [5, 17] are kept common amongst the 32 cases. The number of computational cells for all cases was 400, and to maintain the same level of accuracy, the mean free path was kept at approximately 25 μm by varying the input pressure with the input temperature. With a domain length of 1 mm, the ratio of cell width to mean free path was maintained at approximately 0.1 for all cases. The Knudsen number, which is a ratio of the mean free path to domain length, is therefore approximately 0.025. Likewise, the time step was chosen for each case such that it was always 10% of the mean collision time. 40,000 particles were used and steady-state sampling began after 300,000 time steps. Bird's [5] values of $\omega_{or} = 0.81$ and $\alpha_{or} = 1.4$ for Ar are widely accepted within the DMSC community and are therefore used herein for the VSS model. For the L-J model, the values of $\sigma_{or} = 3.418$ and $\varepsilon_{or}/k = 124$ K for Ar may be found in Hirschfelder *et al.* [10] and are used herein. In this paper, this set of VSS and L-J model parameters are termed, "original", data set and are used for the 32 cases simulated with P_{or} pressures. The recalibrated values are $\omega_{re} = 0.73$ and $\alpha_{re} = 1.4$ for VSS, and $\sigma_{re} = 3.350$ and $\varepsilon_{re}/k = 150$ K for the L-J models. These values are used for the theoretical viscosity and thermal conductivity calculations in the following section. A list of all necessary input parameters for the 32 cases are categorized into physical and numerical parameters as shown in Table 2.

In the sections that follow, reported average viscosity and thermal conductivity values are averaged over the central 60% of the domain. The sampled viscosities and thermal conductivities have statistical errors inherent to the DSMC method, but are estimated to be below 0.2% and 0.3% for viscosity and thermal conductivity, respectively.

Viscosity and Thermal Conductivity Using Original Parameters

Both theoretical and DSMC results for viscosity and thermal conductivity calculations are presented in this section using the original parameters. Theoretical viscosities and thermal conductivities are computed for argon gas using both VSS and LJ models according to Eqs. (3), (5), and $k = 15k\mu/4m$. Figure 3 shows the theoretical variation of viscosity with temperature for the two models along with the experimental fit of Maitland and Smith [14]. The LJ model is

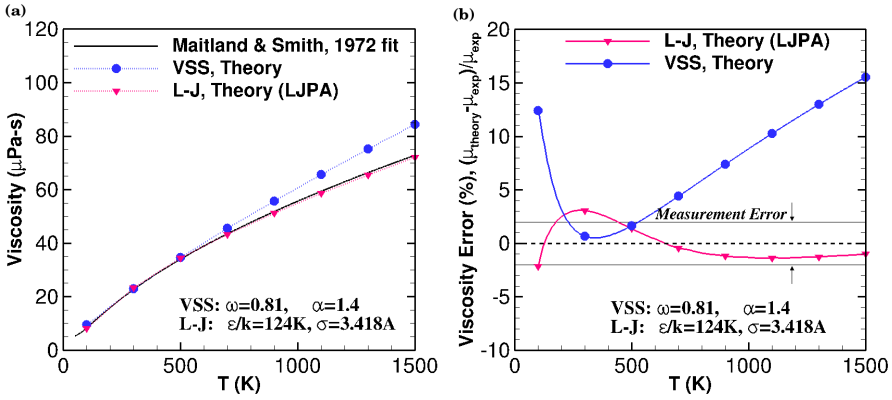

FIGURE 3. (a) Theoretical viscosity variation with temperature using VSS and LJ models and experimental fit of Maitland and Smith [14] (b) Theoretical viscosity errors of VSS and LJ models relative to experimental fit.

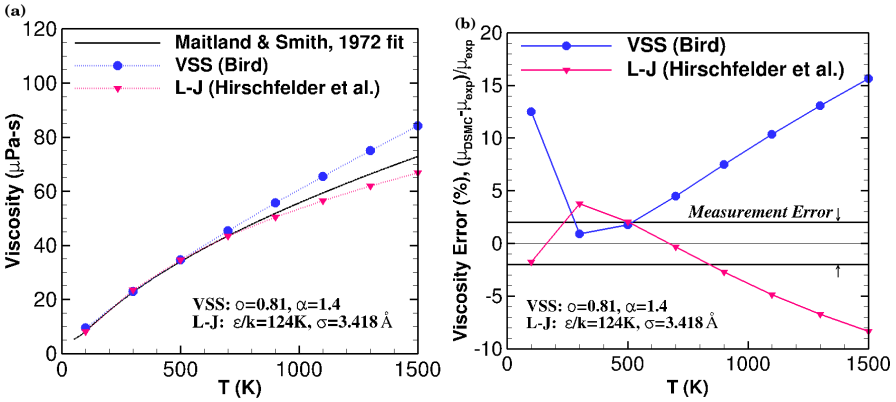

FIGURE 4. (a) DSMC viscosity variation with temperature using VSS and LJ models and experimental fit of Maitland and Smith [14] (b) DSMC viscosity errors of VSS and LJ models relative to experimental fit.

observed to be in much better agreement with the experimental fit overall, with a maximum error less than 4%. The VSS model is only sufficiently accurate near its reference temperature of 273 K and at lower and higher temperatures the error increases to more than 10%.

Viscosities computed from DSMC simulations of Couette flow are illustrated in Fig. 4 along with the experimental fit of Maitland and Smith [14]. The LJ model is still in good agreement with experiments up until near 900 K where it begins to deviate. This is in contrast to theoretical results which had shown LJ to be within the $\pm 2\%$ measurement error beyond 500 K. It is not yet clear why this discrepancy between DSMC and theory should exist, given the accuracy of the collision frequency calculations at high temperatures presented in Section . One possibility is insufficient number of simulated particles for the LJ model. At higher temperatures, more collisions occur (more so for LJ than VSS) and it may be necessary to increase the number of simulated particles in order to ensure molecular chaos.

Thermal conductivity varies linearly with viscosity and so follows a similar trend. Figure 5 shows the theoretical variation of thermal conductivity with temperature using VSS and LJ models and a linear interpolation of experimental measurements [12,13] [18, 19, 20, 21, 22, 23]. Again, the LJ model more accurately predicts the thermal conductivity - being within the $\pm 2\%$ measurement error beyond 500 K.

Thermal conductivities obtained from DSMC simulations of Fourier flow are shown in Fig. 6. As with viscosity calculations, the DSMC results for thermal conductivity deviate from theory at higher temperatures. With this behavior, neither LJ nor VSS models are within the measurement error beyond 900 K.

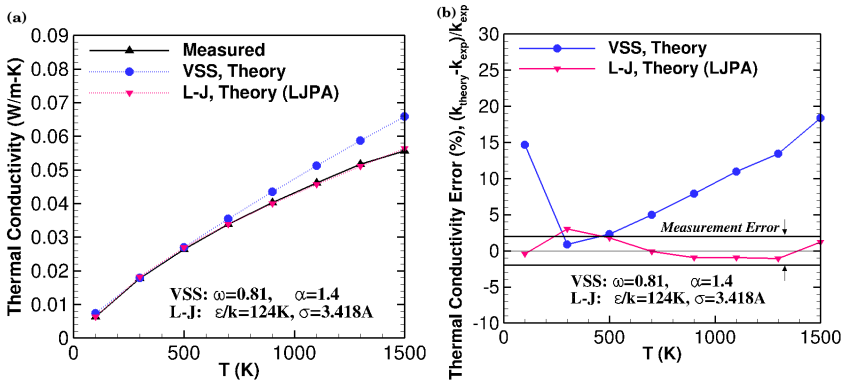

FIGURE 5. (a) Theoretical thermal conductivity variation with temperature using VSS and LJ models and interpolation of experimental measurements (b) Theoretical thermal conductivity errors of VSS and LJ models relative to interpolation of experimental measurements.

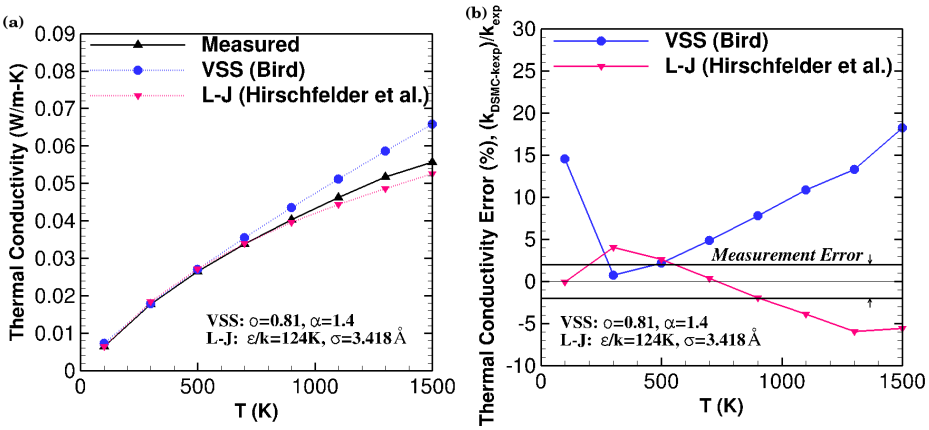

FIGURE 6. (a) DSMC thermal conductivity variation with temperature using VSS and LJ models and interpolation of experimental measurements (b) DSMC thermal conductivity errors of VSS and LJ models relative to interpolation of experimental measurements.

Viscosity and Thermal Conductivity Using Recalibrated Parameters

The results of the previous subsection are useful in that they compare the performances of the molecular models using widely accepted parameter values; however, the comparison to the experimental data set of this study is not the same set as the parameters were determined. This presents an issue of isolating the effect of the choice of model parameters from the model itself. To resolve this issue, the model parameters are recalibrated according to the experimental data set of this study using the theoretical expressions provided in Section .

Comparing the viscosities and thermal conductivities computed from theory to the measurements in Figure 7 shows much better agreement - especially for the VSS model. While both the VSS and L-J models mostly remain within the $\pm 2\%$ measurement error, the L-J model remains within 1.4% for temperatures above and including 300 K. The VSS model, with the exception of the simulation at 100 K, varies between –3.0 and +2% and is more rapidly diverging from the measured values towards the higher temperatures. Both the L-J and VSS models have local maximum/minimum at 500 K, with the magnitude of the VSS model error being a factor of two greater than that of the L-J model.

CONCLUSIONS

Effects of intermolecular interaction models are evaluated in DSMC through the analysis of Couette and Fourier flows. The theory of polynomial approximations was used to represent the scattering angle for the LJ potential using a two-variable polynomial of degree 7. The formulation for the scattering angle was first verified via equilibrium

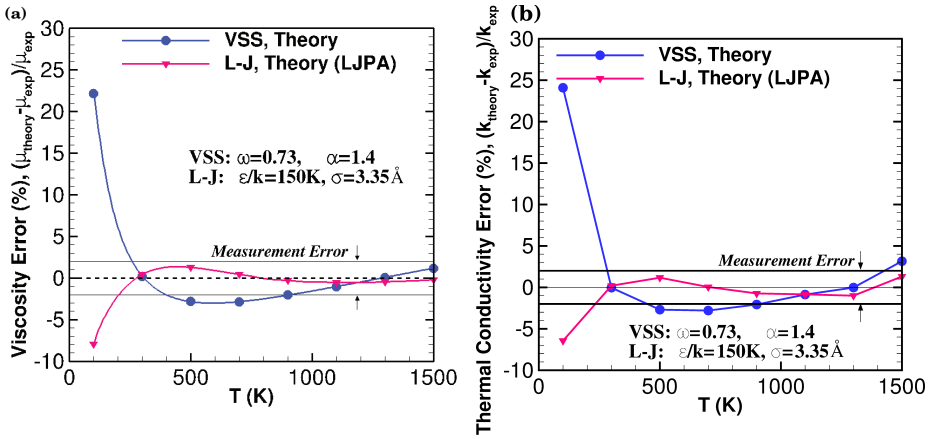

FIGURE 7. Comparison of VSS and L-J models using recalibrated parameters in temperature range 100–1,500 K for argon gas (a) theoretical viscosity errors and (b) theoretical thermal conductivity errors.

collision frequency calculations for argon.

Theoretical calculations of viscosity and thermal conductivity using model parameters typically found in literature show the LJ model to be in better agreement with experimental measurements than the VSS model. LJ has a maximum viscosity error of less than 4% and remains within the measurement error beyond 500 K; while the VSS model is only within the measurement error between 230 and 530 K.

DSMC simulations of Couette and Fourier flow result in viscosities and thermal conductivities which deviate from theory for the LJ model. One possible explanation for this discrepancy is insufficient number of simulated particles per cell. The LJ model has a higher collision frequency relative to the VSS model and this increases with temperature. As a result of, the assumption of molecular chaos may break down within the DSMC collision procedure.

Recalibrating the model parameters has a significant impact on the model performance, VSS model especially. The range of validity for the VSS model relative to argon gas viscosity measurements was extended from 230–530 K up to 1,650 K. New parameters for a wide temperature range for argon and molecular nitrogen gases have been suggested.

REFERENCES

1. W. Louisos, A. Alexeenko, D. Hitt, and A. Zilic, *Int. J. Manuf. Res.* **3**, 80–113 (2008).
2. M. Gallis, and J. Torczynski, *Microelectromechanical Systems, Journal of* **13**, 653–659 (2004).
3. M. Ivanov, and S. Gimelshein, *Annual Review of Fluid Mechanics* **30**, 469–505 (1998).
4. G. LeBeau, *Computer methods in applied mechanics and engineering* **174**, 319–337 (1999).
5. G. A. Bird, *Molecular Gas Dynamics and the Direct Simulation of Gas Flows*, Oxford University Press, New York, 1994, 2nd revised edn.
6. K. Koura, and H. Matsumoto, *Physics of Fluids A: Fluid Dynamics* **3**, 2459 (1991).
7. F. Sharipov, and J. L. Strapasson, *Physics of Fluids* **24**, 011703 (2012).
8. A. Venkattraman, and A. Alexeenko, *Physics of Fluids* **24**, 027101 (2012).
9. J. O. Hirschfelder, R. B. Bird, and E. L. Spotz, *Journal of Chemical Physics* **16(10)**, 968–981 (1948).
10. J. O. Hirschfelder, C. F. Curtiss, and R. B. Bird, *Molecular Theory of Gases and Liquids*, Wiley, New York, 1954.
11. J. Kestin, S. Ro, and W. Wakeham, *J. Chem. Phys.* **56**, 4119–4124 (1972).
12. E. May, R. Berg, and M. Moldover, *Int. J. Thermophys.* **28**, 1085–1110 (2007).
13. E. Vogel, B. Jäger, R. Hellmann, and E. Bich, *Molecular Physics* **108**, 3335–3352 (2010).
14. G. Maitland, and E. Smith, *Journal of Chemical and Engineering Data* **17**, 150–156 (1972).
15. H. Matsumoto, and K. Koura, *Physics of Fluids A: Fluid Dynamics* **3**, 30–38 (1991).
16. G. A. Bird, *The DSMC Method*, G. A. Bird, Sydney, 2013, ISBN 9781492112907.
17. W. Vincenti, and J. Kruger, C.H., *Introduction to Physical Gas Dynamics*, Wiley, New York, NY, 1965.
18. W. Kunnuluik, and E. Carman, *Proc. Phys. Soc. B.* **65**, 701–709 (1952).
19. F. M. Faubert, and G. S. Springer, *J. Chem. Phys.* **57**, 2333–2340 (1972).
20. H. Hanley, *J. Chem. Phys. Ref. Data* **2**, 619–642 (1973).
21. S. Chen, and S. Saxena, *Molecular Physics* **29**, 455–466 (1975).
22. J. Kestin, R. Paul, A. Clifford, and W. Wakeham, *Physica A.* **100**, 349–369 (1980).
23. H. M. Roder, R. A. Perkins, and A. Laesecke, *J. Res. NIST* **105**, 221–253 (2000).